NeuroImage 86 (2014) 111–122

Contents lists available at ScienceDirect

NeuroImage

journal homepage: www.elsevier.com/locate/ynimg

SPoC: A novel framework for relating the amplitude of neuronal oscillations to behaviorally relevant parameters

Sven Dähne [a,d,*], Frank C. Meinecke [a], Stefan Haufe [a,b], Johannes Höhne [a], Michael Tangermann [a], Klaus-Robert Müller [a,b,c,d,e,**], Vadim V. Nikulin [c,d,***]

[a] Machine Learning Group, Department of Computer Science, Berlin Institute of Technology, Marchstr. 23, 10587 Berlin, Germany
[b] Bernstein Focus Neurotechnology, Berlin, Germany
[c] Neurophysics Group, Department of Neurology, Campus Benjamin Franklin, Charité University Medicine Berlin, 12203 Berlin, Germany
[d] Bernstein Center for Computational Neuroscience, Berlin, Germany
[e] Department of Brain and Cognitive Engineering, Korea University, Anam-dong, Seongbuk-gu, Seoul 136-713, Republic of Korea

ARTICLE INFO

Article history:
Accepted 30 July 2013
Available online 15 August 2013

Keywords:
EEG
MEG
Oscillations
SPoC
Source power comodulation
ASSEP

ABSTRACT

Previously, modulations in power of neuronal oscillations have been functionally linked to sensory, motor and cognitive operations. Such links are commonly established by relating the power modulations to specific target variables such as reaction times or task ratings. Consequently, the resulting spatio-spectral representation is subjected to neurophysiological interpretation. As an alternative, independent component analysis (ICA) or alternative decomposition methods can be applied and the power of the components may be related to the target variable. In this paper we show that these standard approaches are suboptimal as the first does not take into account the superposition of many sources due to volume conduction, while the second is unable to exploit available information about the target variable. To improve upon these approaches we introduce a novel (supervised) source separation framework called Source Power Comodulation (SPoC). SPoC makes use of the target variable in the decomposition process in order to give preference to components whose power comodulates with the target variable. We present two algorithms that implement the SPoC approach. Using simulations with a realistic head model, we show that the SPoC algorithms are able extract neuronal components exhibiting high correlation of power with the target variable. In this task, the SPoC algorithms outperform other commonly used techniques that are based on the sensor data or ICA approaches. Furthermore, using real electroencephalography (EEG) recordings during an auditory steady state paradigm, we demonstrate the utility of the SPoC algorithms by extracting neuronal components exhibiting high correlation of power with the intensity of the auditory input. Taking into account the results of the simulations and real EEG recordings, we conclude that SPoC represents an adequate approach for the optimal extraction of neuronal components showing coupling of power with continuously changing behaviorally relevant parameters.

Introduction

Neural oscillations as measured by electro- and magnetoencephalography (EEG/MEG) have long been associated with sensory, motor, as well as cognitive processing (Buzsáki and Draguhn, 2004) and information transfer within the brain (Colgin et al., 2009; Womelsdorf and Fries, 2007).

In particular, it is widely believed that the amplitude/power modulation of these oscillations reflects the amount of spatial synchronization among neurons corresponding to different brain states (see (Rieder et al., 2011) for a review).

Cognitive phenomena, that have been shown to correlate with band power modulations, include e.g. attention (Başar et al., 1997; Bauer et al., 2006; Brovelli et al., 2005; Debener et al., 2003; Haegens et al., 2011a; Kaiser et al., 2006; Klimesch et al., 1998; Tallon-Baudry et al., 2005), memory encoding (Jensen et al., 2007; Klimesch, 1999; Osipova et al., 2006), vigilance in operational environments (Gevins et al., 1995; Holm et al., 2009), sleep stages (Darchia et al., 2007; Demanuele et al., 2012), perception (Gonzalez Andino et al., 2005; Jin et al., 2006; Makeig and Jung, 1996; Plourde et al., 1991; Thut et al., 2006), and decision making (Haegens et al., 2011a, 2011b). In Transcranial Magnetic Stimulation research it has also been shown that the excitability of the

* Correspondence to: S. Dähne, Machine Learning Group, Department of Computer Science, Berlin Institute of Technology, Marchstr. 23, 10587 Berlin, Germany.
** Correspondence to: K.-R. Müller, Bernstein Focus Neurotechnology, Berlin, Germany.
*** Correspondence to: V.V. Nikulin, Neurophysics Group, Department of Neurology, Campus Benjamin Franklin, Charité University Medicine Berlin, 12203 Berlin, Germany.
E-mail addresses: sven.daehne@tu-berlin.de (S. Dähne), klaus-robert.mueller@tu-berlin.de (K.-R. Müller), vadim.nikulin@charite.de (V.V. Nikulin).

1053-8119
http://dx.doi.org/10.1016/j.neuroimage.2013.07.079

motor (Sauseng et al., 2009) and visual cortices (Romei et al., 2008), measured in terms of the amplitude of alpha oscillations, can also be predictive of muscular motor evoked potentials and visual perception, respectively. In the field of Brain–Computer Interfaces (BCI), voluntary modulation of EEG band power is used to control computer applications, such as text entry systems (Blankertz et al., 2007, 2008). It has been shown recently that variability in BCI control-performance can be partially explained by the variability of spectral power across subjects (Blankertz et al., 2010), as well as within subjects (Grosse-Wentrup et al., 2011; Maeder et al., 2012).

For the purpose of this paper, we introduce the concept of a *target variable* (in the following denoted by z), which in principle can be any scalar function of time. In the present neuroscience context, this target variable will typically represent a behavioral measure as the final output of the central nervous activity (e.g. reaction time, sensory detection, task rating, motor evoked potentials, etc.) or parameters of external stimuli (e.g. when studying how amplitude modulation of neuronal oscillations correlates with stimulus properties).

In general, we want to investigate the relation between EEG/MEG spectral power and such z variable in order to find a possible functional relationship between neuronal amplitude modulations and a behavior or stimulus. There are two standard approaches for establishing this relationship. In the first one, the spectral power is computed for each channel/sensor. A correlation to the target variable is then either assessed per channel, or using a multivariate regression approach. In the second approach, a linear projection from a sensor space into so-called source space is performed and further processing is performed therein. As we will show later in detail, neither of the two common approaches can be expected to yield optimal performance with EEG/MEG data both in terms of the maximized correlation scores and the accuracy with which the underlying sources are extracted, thus limiting the subsequent neurophysiological interpretation of the results.

This paper explains the drawbacks of the conventional analyses and suggests the novel Source Power Comodulation (SPoC) framework, which provides a theoretically sound and mathematically optimal solution to the problem of relating EEG/MEG data to a given target variable.

The remainder of this article is organized as follows. In the Methods section we recall the EEG/MEG forward model, discuss standard approaches to obtaining correlations between band power and a target variable, and thereafter introduce the SPoC framework and two specific SPoC algorithms. The new approach is validated in simulations and with real world data, both described in the Validation section. Results are presented in the Results section and we conclude with a discussion in the Discussion section.

Methods

The generative model of EEG/MEG data

Electro- and magnetoencephalography are non-invasive techniques allowing to measure macroscopic neuronal activity of the brain. While EEG measures scalp electrical potentials caused by neuronal activity, MEG measures the corresponding magnetic fields. Due to the volume conduction in the head, the neuronal signals are spatially smeared while propagating to the EEG/MEG sensors. For the frequencies of interest in the analysis of brain oscillations (which are typically below 1 kHz) this superposition is linear and instantaneous (Baillet et al., 2001; Nunez and Srinivasan, 2006; Parra et al., 2005). Thus, the following linear model holds for EEG/MEG data:

$$\mathbf{x}(t) = \mathbf{A}\mathbf{s}(t) + \epsilon(t). \tag{1}$$

The vector $\mathbf{x}(t) \in \mathbb{R}^{N_x}$ here denotes the measured data in sensor space (electrical potential or magnetic field) at time t, with N_x being the number of recording channels. The measurement is a linear superposition of N_s sources (or components) with individual time courses $s_i(t)$ and fixed spatial patterns $\mathbf{a}^i \in \mathbb{R}^{N_x}$, where $\mathbf{s}(t) = (s_1(t), \ldots, s_{N_s}(t))^\top$ contains the time courses of the individual sources, $\mathbf{A} = (\mathbf{a}^1, \ldots, \mathbf{a}^{N_s})$ contains the respective spatial patterns in the columns, and $\epsilon(t)$ models additive noise. Generally, the time courses of the sources are assumed to be uncorrelated and to have unit variance. Furthermore, the noise term can be absorbed into the product **As** by adding additional columns in **A** and respective dimensions in **s**. Therefore we will omit the noise term in the following considerations.

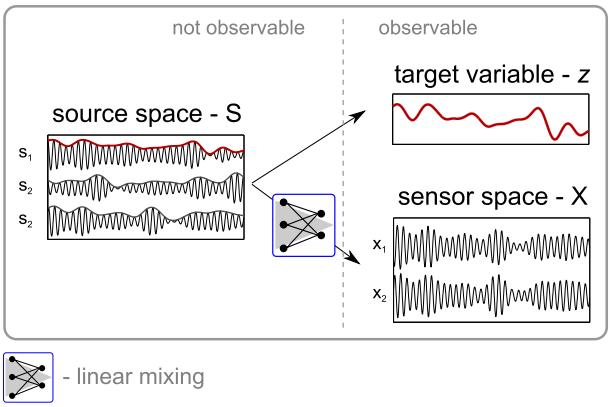

Fig. 1. Illustration of the problem setting. The unobservable source space signals (e.g. oscillatory brain sources) are mixed to constitute the sensor space signals (e.g. EEG/MEG). The time course of the observed target variable z (e.g. stimulus intensity, reaction times) corresponds to the power (or envelope) modulation of one of the sources.

Here we are interested in neural oscillations whose power time course comodulates (e.g. is correlated or anti-correlated) with an external variable. These neural oscillations are however not unambiguously observable on the sensor level. Instead, they are superimposed with the background brain activity and noise according to Eq. (1). This problem setting is illustrated in Fig. 1.

Conventional approaches

Correlating the power of single sensors

Due to the source mixing, each sensor signal is generally a linear sum of (1) the signal-of-interest s, whose power correlates with the target variable z and (2) noise[1] sources n, whose power does not correlate with the target. This implies that the correlation between z and the band power at any electrode is in fact a correlation between the power of s with z, normalized by a term that grows monotonically with the squared mixing coefficients of both the signal and noise sources, as well as with the variances of their band power time courses (see Appendix A). This illustrates the major drawbacks of the univariate approach:

- *Low signal-to-noise ratio*. The true correlation between the power of s and z may be heavily underestimated in the presence of strong noise sources with high power.
- *Lack of interpretability*. The noise contribution may differ across electrodes, introducing a channel-specific bias in the correlation coefficients. Hence, topographic maps of sensor-space correlation may not give a good indication of where the signal-of-interest is strongest and are thereby hard to interpret in neurophysiological terms.
- *Disregard of the generative model*. It is practically impossible to disentangle signal and noise contributions by looking only at single electrodes. More generally, this approach does not provide a factorization of the measurement $\mathbf{x}(t)$ into **A** and $\mathbf{s}(t)$ according to the generative linear model of EEG/MEG data (see Eq. (1)).

[1] The term *noise sources* subsumes all signals whose power is not related to the target variable. Specifically, this also includes actual brain sources which are different from e.g. measurement noise.

Correlating linear combinations of sensor power

Instead of correlating the band power of individual channels with z, multivariate approaches can be applied, in which the target variable z is correlated with a weighted sum of the channel-wise band power. Usually, the weights are chosen by regressing the band-power with the target variable, thereby effectively maximizing the correlation. Using this approach, it is generally possible to achieve a high correlation (on the data used to train the weight vector) if a sufficient amount of training data is available. This may achieve superior performance compared to univariate correlation in low signal-to-noise scenarios, thereby improving upon the first point in the list above. However, in principle the other two drawbacks remain:

- *Lack of interpretability*. The regression weight vector does not necessarily contain neurophysiologically interpretable information about the location of the underlying correlating source, because it is again a function of both the signal-of-interest and the noise (an explanation for this can be found in (Blankertz et al., 2011)).
- *Disregard of the generative model*. Linearly regressing power values violates the underlying generative model for EEG and MEG data, because it is linear in the 'raw' data, not in the squared data.

Blind source separation methods

A transformation into source space can be obtained by way of so-called blind source separation methods (BSS). These methods usually estimate a linear projection of the data $\mathbf{x}(t)$ onto a set of weight vectors, which are represented here by the matrix $\mathbf{W}\in\mathbb{R}^{N_x\times N_{\hat{s}}}$, where $\mathbf{W}=(\mathbf{w}^1,\ldots,\mathbf{w}^i,\ldots,\mathbf{w}^{N_{\hat{s}}})$, $\mathbf{w}^i\in\mathbb{R}^{N_x}$, and $N_{\hat{s}}$ corresponds to the number of estimated sources $\hat{s}_i(t)$. In accordance with the literature, we refer to these weight vectors $\mathbf{w}^i$ as *spatial filters*. Each of the spatial filters is meant to extract the signal from one source while suppressing the activity of the others, such that the resulting projected signal is a close approximation of the original source signal, i.e. $\hat{s}_i(t)=\mathbf{w}^{i\top}\mathbf{x}(t)$. Band power correlations are then computed using $\hat{s}_i(t)$ instead of $x_k(t)$. Popular BSS approaches, such as ICA, are in line with the generative model of EEG/MEG and can thus in principle deliver results that are interpretable within this model.

Note however that, by design, BSS methods are unsupervised learning methods. They do not make use of a target variable z but optimize other objectives instead, such as statistical independence, for example. This lack of optimizing for the desired target z leads to a suboptimal performance of BSS methods if:

- There is a *low signal-to-noise ratio*,
- There are *more sources than channels*,
- *The target and the independence assumption contradict one another* due to dependencies between the sources.

The SPoC approach

The core idea of the SPoC framework is to (i) decompose the multivariate EEG/MEG data into a set of source components and (ii) to use the information contained in the target variable to guide the decomposition. The result of this approach is a set of spatial filters, $\mathbf{W}$, which *directly* optimize the comodulation between the target variable z and the power time course of the spatially filtered signal. Fig. 2 illustrates the contrast between regression of channel-wise band power features, BSS methods, and the SPoC approach.

In the following subsection, we describe two algorithms that implement the SPoC framework and we refer to these two methods as SPoC_{r2} and SPoC_{λ}. The difference between SPoC_{r2} and SPoC_{λ} lies in the exact definition of comodulation between band power and z: SPoC_{r2} directly optimizes correlation, while SPoC_{λ} optimizes covariance subject to a scaling constraint on the spatial filter. However, both algorithms invert the generative model given in Eq. (1) *prior* to the computation of band power and thereby avoid pitfalls that were outlined above.

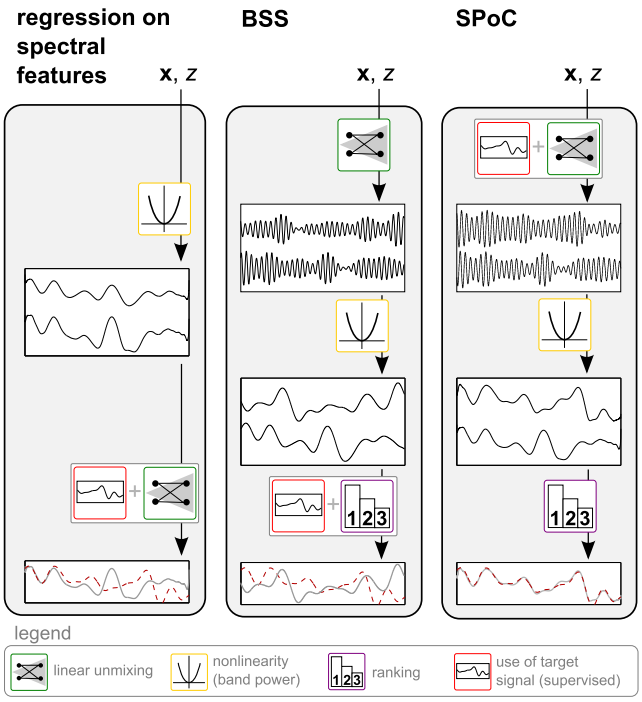

Fig. 2. Illustration of different approaches to relating spectral power to a target variable. The input to all three approaches is the EEG/MEG data $\mathbf{x}(t)$ and the target variable z. Processing steps are organized from top to bottom. Left: an approach that is based on regression. First, spectral power is computed on each sensor. Then the power time courses are linearly combined to resemble z as close as possible. Middle: an approach that is based on blind source separation (BSS) methods. A BSS method such as ICA tries to estimate the sources prior to computation of spectral power. This approach is in line with the generative EEG model and in principle could have the potential to find the true source. However, BSS techniques do not make use of the information contained in z and is bound to fail for low SNR or if the number of sources is larger than the number of channels. Right: Our novel SPoC approach method makes use of z to guide the source estimation and to give preference to sources whose power time course resembles z. Spectral power is computed on the estimated *sources*.

The SPoC algorithms

This subsection describes two possible ways to implement the SPoC idea outlined above. While the following definitions and derivations are important for understanding how the actual SPoC algorithms work, the mathematically less inclined reader may skip ahead to the Validation section without missing out on the main message of this paper.

Assumptions and definitions

We assume that the EEG/MEG data $\mathbf{x}(t)$ has been band-pass filtered in the frequency band of interest already. Thus, the power of the projected signal $\mathbf{w}^\top\mathbf{x}(t)$ within a given time interval is well approximated by the variance of $\mathbf{w}^\top\mathbf{x}(t)$ within that interval. We refer to such time intervals as *epochs* and assume that the EEG/MEG data can be divided up into consecutive or overlapping epochs of suitable length.[2] Epochs will be indexed by the index e.

We assume the target variable z to only have a single value per epoch, which can be achieved by appropriate resampling. Furthermore we assume without loss of generality that z has zero mean and unit variance, which can be achieved by normalization.

It is our goal to approximate the target variable z with a quantity that we denote by $\tilde{z}$, which depends on a spatial filter $\mathbf{w}$. Let $Var[\mathbf{w}^\top\mathbf{x}(t)](e)$

[2] Working with epoched data instead of continuous data does not represent a loss of generality, because all of the following derivations can be reformulated for continuous data as well, provided that the target variable changes slowly enough. We choose to work with epoched data because it resembles the format of data obtained in trial-based experiments.

denote the variance of $\mathbf{w}^\top\mathbf{x}(t)$ in a given epoch e. This epoch-wise variance of the projected signal will serve as the approximation of z. However, in the following we will slightly modify this quantity such that it has zero mean by definition. First, we note that $Var[\mathbf{w}^\top\mathbf{x}(t)](e) = \mathbf{w}^\top\mathbf{C}(e)\mathbf{w}$, where $\mathbf{C}(e)$ denotes the covariance matrix of $\mathbf{x}(t)$ in the eth epoch. Then we define the mean covariance matrix

$$\mathcal{C} := \langle \mathbf{C}(e) \rangle, \tag{2}$$

where $\langle\cdot\rangle$ denote the average across epochs. With these definitions we can now define our quantity of interest as

$$\begin{aligned} \tilde{z}(e) &:= Var\left[\mathbf{w}^\top\mathbf{x}(t)\right](e) - \mathbf{w}^\top\mathcal{C}\mathbf{w} \\ &= \mathbf{w}^\top(\mathbf{C}(e) - \mathcal{C})\mathbf{w}. \end{aligned} \tag{3}$$

Accordingly, the first two moments of $\tilde{z}$ can be expressed in terms of the weight vector and epoch-wise covariance matrices as:

$$\begin{aligned} \langle \tilde{z}(e) \rangle &= \left\langle \mathbf{w}^\top(\mathbf{C}(e) - \mathcal{C})\mathbf{w} \right\rangle \\ &= {}^\top\langle \mathbf{C}(e) \rangle \mathbf{w} - \mathbf{w}^\top\mathcal{C}\mathbf{w} \\ &= \mathbf{w}^\top\mathcal{C}\mathbf{w} - \mathbf{w}^\top\mathcal{C}\mathbf{w} \\ &= 0 \end{aligned} \tag{4}$$

and

$$\begin{aligned} Var\left[\tilde{z}(e)\right] = &\left\langle \left(\tilde{z}(e) - \langle \tilde{z}(e) \rangle\right)^2 \right\rangle \\ &\left\langle \left(\mathbf{w}^\top(\mathbf{C}(e) - \mathcal{C})\mathbf{w}\right)^2 \right\rangle. \end{aligned} \tag{5}$$

Finally, we define the matrix

$$\mathcal{C}_z := \langle \mathbf{C}(e) z(e) \rangle, \tag{6}$$

which helps to conveniently express the covariance between $\tilde{z}$ and z as

$$\begin{aligned} Cov\left[\tilde{z}(e), z(e)\right] &= \left\langle \left(\tilde{z}(e) - \langle \tilde{z}(e) \rangle\right)\left(z(e) - \langle z(e) \rangle\right) \right\rangle \\ &= \left\langle \left(\mathbf{w}^\top(\mathbf{C}(e) - \mathcal{C})\mathbf{w}\right) z(e) \right\rangle \\ &= \mathbf{w}^\top \langle \mathbf{C}(e) z(e) \rangle \mathbf{w} - \left(\mathbf{w}^\top\mathcal{C}\mathbf{w}\right) \langle z(e) \rangle \\ &= \mathbf{w}^\top \mathcal{C}_z \mathbf{w}, \end{aligned} \tag{7}$$

where in the transition from line 1 to line 2 of this equation we have used the fact that $\langle \tilde{z}(e) \rangle = \langle z(e) \rangle = 0$ and substituted the definition for $\tilde{z}(e)$. The next line is the result of factoring out. Finally, we made use of $\langle z(e) \rangle = 0$ again and applied the definition for $\mathcal{C}_z$, given in Eq. (6).

In the following subsections we formulate the objectives optimized by the two algorithms that implement the SPoC approach. For ease of notation, the derivations are given for a single weight vector $\mathbf{w} \in \mathbb{R}^{N_x}$, but generalize naturally to multiple filters providing a full-rank decompositions of the data matrix.

Optimizing source power correlation

We are interested in positive as well as negative correlations and hence choose to maximize the squared correlation between z and $\tilde{z}$. We refer to this SPoC algorithm as SPoC_{r2} and maximize the following objective function:

$$\begin{aligned} f_{\text{r2}} &= Corr\left[\tilde{z}(e), z(e)\right]^2 \\ &= \frac{Cov\left[\tilde{z}(e), z(e)\right]^2}{Var\left[\tilde{z}(e)\right] Var\left[z(e)\right]} \\ &= \frac{\left(\mathbf{w}^\top\mathcal{C}_z\mathbf{w}\right)^2}{\left\langle \left(\mathbf{w}^\top(\mathbf{C}(e) - \mathcal{C})\mathbf{w}\right)^2 \right\rangle}. \end{aligned} \tag{8}$$

In the last equality of Eq. (8) we have used Eqs. (7) and (5), and the fact that $Var[z(e)] = 1$.

The weight vector $\mathbf{w}$ that maximizes f_{r2} cannot be found analytically. It should therefore be found using iterative optimization methods such as gradient descent for example.

Optimizing source power covariance

Here we approximate the previous objective function by optimizing the covariance between $\tilde{z}$ and z. As we will show shortly, this leads to an objective function that has a number of computationally desirably properties. We refer to this algorithm as SPoC_λ. Unlike the correlation, the covariance is affected by the scaling of its arguments. Thus far we have assumed z to have zero mean and unit variance, i.e. that the scaling of z is limited. Since we have only assumed $\tilde{z}$ to have zero mean, it is furthermore necessary to limit the scaling of $\tilde{z}$. In SPoC_λ we impose a constraint on the norm of $\mathbf{w}$ and thereby limit the scaling of $\tilde{z}$. Specifically we choose the constraint such that the output of the spatial filter has unit variance. With these definitions we arrive at the following objective function:

$$f_\lambda = Cov\left[\tilde{z}(e), z(e)\right] = \mathbf{w}^\top\mathcal{C}_z\mathbf{w}, \tag{9}$$

with respect to the following norm constraint:

$$Var\left[\mathbf{w}^\top\mathbf{x}(t)\right] = \mathbf{w}^\top\mathcal{C}\mathbf{w} \stackrel{!}{=} 1. \tag{10}$$

This constraint optimization problem can be solved using the method of Lagrange multipliers. Setting the first derivative of the corresponding Lagrangian to zero leads to the following generalized eigenvalue equation:

$$\mathcal{C}_z\mathbf{w} = \lambda\mathcal{C}\mathbf{w}, \tag{11}$$

where the eigenvalue λ corresponds to the value of f_λ evaluated at the respective eigenvector $\mathbf{w}$. Thus λ can directly be interpreted as the covariance between $\tilde{z}$ and z.

Finding the solution to optimizing f_λ is not as time consuming as iterative optimization procedures and the obtained solution is unique, i.e. no restarts are necessary. Furthermore, the result of solving the generalized eigenvalue problem is a full set of weight vectors, i.e. a matrix $\mathbf{W}$ with the eigenvectors in its columns. This matrix contains a column vector $\mathbf{w}$ that *maximizes* f_λ as well as a different column $\mathbf{w}$ that *minimizes* the same objective function. After sorting the columns of $\mathbf{W}$ according to their respective eigenvalues, one finds these weight vectors in the first and last column of $\mathbf{W}$. The matrix $\mathbf{W}$ has full rank but its columns are *not* mutually orthogonal, as is the case in PCA for example.

Spatial patterns

Our modeling approach (i.e. the SPoC objective functions) allows for a meaningful interpretation of the results. Since we are seeking a linear spatial filter $\mathbf{w}$, we are able to derive the corresponding spatial pattern, which we denote with the vector $\mathbf{a}$. By spatial patterns we refer to the columns of the mixing matrix $\mathbf{A}$ (see Eq. (1)), which can, for example, be obtained by inverting the full filter matrix $\mathbf{W}$. If the full filter matrix is not available, estimates for a spatial pattern $\mathbf{a}$ corresponding to individual spatial filter $\mathbf{w}$ can be obtained via the relation

$$\begin{aligned} \mathbf{a} &\propto \sum_t \mathbf{x}(t)\left(\mathbf{w}^\top\mathbf{x}(t)\right) \\ &\propto \mathcal{C}\mathbf{w}. \end{aligned} \tag{12}$$

See (Parra et al., 2005) for further details. The spatial pattern of a filter $\mathbf{w}$ can be interpreted as the scalp projection of the source whose activity is extracted via $\mathbf{w}$. In accordance with (Parra et al., 2005) and (Blankertz et al., 2011) we suggest to visualize the spatial patterns rather than the filters in order to interpret the results.

Validation

SPoC is designed to find a spatial filter that extracts an oscillatory signal whose power modulation follows a given target variable. We tested this ability in high dimensional and noisy environments by applying SPoC as well as linear regression and a BSS method (here we used ICA) to simulated as well as real EEG data. In the simulations, the time course of the source signal (and therefore also its power modulation) are known. Thus the results of the methods can be compared to the ground truth. For the real EEG data, we choose an auditory steady state paradigm in which the near linear relationships between stimulus intensity and neuronal amplitude modulations have been reported before (Picton et al., 2003).

Simulated data

Data generation. Simulated 58 channel EEG data was created according to the generative model outlined in The generative model of EEG/MEG data section. The mixing matrix **A** and the source time courses **s** were created separately. For **A** we used realistic spatial patterns obtained from placing dipoles with random orientations at random locations in a head model and then computing the respective scalp projections. Oscillatory source time courses with controlled spectra and known band power modulations were created using the inverse Fourier transform. A single target source and 100 background sources were created in this manner and the SNR between them is controlled by a parameter, which we denote by γ. See the Appendix of this manuscript for a detailed account on how the simulated data was generated and how the SNR is controlled.

In a given simulation run, a total of 850 s (i.e. approximately 9 min) of data were simulated. Using an epoch length of 1 s, the data was segmented into 850 non-overlapping epochs. Of this data, the first 250 epochs were used for training the algorithms, while the remaining 600 epochs we used for testing. The training signal for linear regression and the two SPoC algorithms consisted of the power time course of the target source.

In order to assess the robustness of the algorithm with respect to noise, the outlined simulation procedure was repeated for different levels of the SNR parameter γ, while keeping the amount of data constant (i.e. 250 training and 600 test epochs). For each value of γ, the simulations were repeated 500 times, each time with newly created data (i.e. new source time courses and new patterns). Thereby a distribution of correlation values was obtained for each of the methods at each SNR level.

Furthermore, the effect of the amount of available training data at a fixed SNR level was investigated.

The SNR level used in these simulations was set to $\gamma = 10^{0.4} \approx 2.5$. The amount of testing epochs was the same as above (600 epochs), but the number of epochs used for training was varied systematically from 10 to 200, in steps of 10. For each number of training epochs, the simulations were repeated 500 times, each time with newly created data, also yielding a distribution of correlation values for each method.

Data analysis. Two metrics were used to quantify the quality of the recovered filter **w**. The first metric was the correlation between the known true power time course z and the estimated power time course $\widetilde{z}$. The second metric was the similarity between the true spatial pattern and the estimated spatial pattern. This similarity was quantified via the absolute value of the spatial correlation between the true and the estimated pattern. Please note that in contrast to $SPoC_{r2}$, $SPoC_{\lambda}$ does not explicitly optimize correlation but covariance instead. However, here we evaluated all algorithms with respect to correlation in order to have a common metric for comparison between them.

For the linear regression, channel-wise variance features of the training and test data were computed. The regression model was fit to the training data and the resulting weights were applied to the test data. It is common practice to use PCA as a preprocessing before ICA. This type of preprocessing for ICA was adopted here as well, retaining enough PCA components to contain 99% of the variance.[3] In the case of ICA and $SPoC_{\lambda}$, an entire set of weight vectors (components) is obtained, and for ICA these resulting components are not ordered a priori. Therefore the estimated target source was identified on the training data as follows: the ICA component whose power time course correlated maximally with the target variable on the training data was chosen for evaluation on the test data. For $SPoC_{\lambda}$, on the other hand, the resulting components were ordered with respect to the respective eigenvalues. After ordering the SPoC component set obtained from the training data, the first component was used for evaluation on the test data. For $SPoC_{r2}$ only one weight vector was obtained by optimizing the respective objective functions on the training data.

Real EEG data

In order to compare the analysis methods on real EEG data, an experiment on steady-state auditory evoked potentials (SSAEPs) (Picton et al., 2003) was conducted with 11 participants, of which $N = 7$ showed a SSAEP. The data from the remaining 4 participants was not used in this analysis.

Experimental paradigm. The auditory stimulus consisted of a sinusoid with a carrier frequency of 500 Hz which was amplitude modulated with a 40 Hz raised cosine, thus resulting in the steady-state modulation. The resulting sound stimulus is referred to as the *steady-state stimulus*. It has been shown that such a stimulus induces a reliable steady state response in the auditory system, i.e. a significant increase in EEG/MEG power at the stimulation frequency (Galambos et al., 1981; Hari et al., 1989; John et al., 2003; Picton et al., 2003; Plourde et al., 1991). The SSAEP literature suggests a positive correlation between the amplitude of the evoked EEG response and the intensity of the steady-state stimulus when measured in decibel (dB) (Plourde et al., 1991; Rodriguez et al., 1986).

In our paradigm, we realized a continuous amplitude modulation of the sound stimulus by multiplying it with a slowly varying function, which we refer to as the *intensity modulation*. This function modulated the loudness of the stimulus between 10 and 35 dB relative to the subject- and ear specific hearing level (HL). The intensity modulation was created by low-pass filtering white noise with a cut-off frequency of 0.05 Hz, which yields a random, yet smoothly varying fluctuation. Before applying the intensity modulation to the sound stimulus, we equalized the histogram of the intensity modulation such that all sound intensity levels appear with equal probability. The beginning and the end of the sound stimulus were faded in/out to minimal intensity using a half cosine window of 10 s duration. Fig. 3 illustrates the experimental setup, including the construction of the sound stimulus.

The experiment consisted of 3 blocks of 5 min continuous stimulation. Between each block, there was a short pause (less than 1 min) for the participants to rest briefly. The sound stimulus was delivered using in-ear headphones and during the EEG recording participants were instructed to relax but keep their eyes open and to focus on the sound.

Data acquisition. EEG signals were recorded using a Fast'n Easy Cap (EasyCap GmbH) with 63 wet Ag/AgCl electrodes placed at symmetrical positions based on the International 10–20 system. Channels were referenced to the nose. Electrooculogram (EOG) signals were recorded in addition but not used in the present context. Signals were amplified using two 32-channel amplifiers (Brain Products) and sampled at 1 kHz.

Data analysis. For the offline analysis in MATLAB, the signals were low-pass filtered with a cutoff frequency of 90 Hz and subsequently down-sampled to 250 Hz. Additionally a notch filter around 50 Hz was applied to attenuate line noise. The down-sampled and notch filtered EEG data were then band pass filtered with a 3 Hz pass band centered on the

[3] ICA without PCA preprocessing was also tested but the resulting performance was worse compared to ICA with PCA preprocessing.

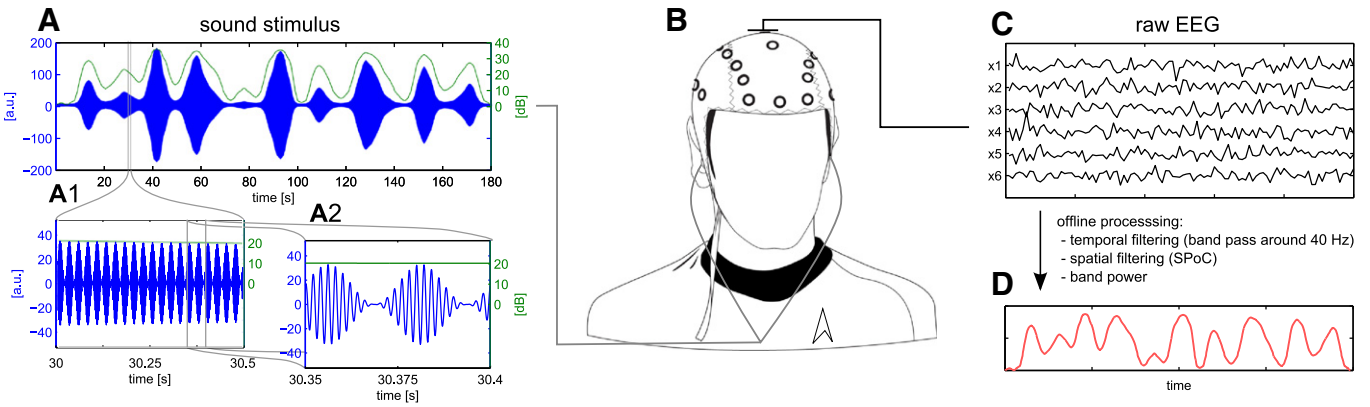

Fig. 3. Auditory stimulus and experimental setup. (A) Three minute excerpt of the intensity modulated steady state stimulus. A 500 Hz sinusoid was multiplied with a 40 Hz raised cosine (see the 0.5 s and 0.05 s excerpts in A1 and A2, respectively). The slowly varying intensity modulation (green line in A, A1, and A2) was applied to the full length steady state stimulus. (B) Participants received the sound stimulus via in-ear headphones and EEG was measured concurrently. (C) The raw EEG was analyzed offline to extract an estimate of the intensity modulation (D).

steady-state frequency of 40 Hz, yielding a pass band from 39 to 41 Hz. The band pass filtered data was then segmented into consecutive epochs of 2 s length and 1 s overlap.

The SSAEP literature suggests a linear relationship between the stimulus intensity (measured in dB) and EEG amplitude at the stimulus frequency. Since the SPoC algorithms and linear regression work on power features (i.e. squared amplitude), we used the *squared* stimulus intensity as the target variable z.

Similar to the analysis on simulated data, a PCA preprocessing (dimensionality reduction, retaining 99% of the variance) was employed for ICA as this improved the results compared to using ICA without PCA preprocessing.

In order the get an unbiased estimate of each of the methods' ability to model the stimulus intensity modulations, we employed a 10-fold chronological cross-validation procedure (Lemm et al., 2011). This means that the whole data was split up into 10 equally sized folds, of which 9 folds served as training data while the remaining fold was used for testing. This training/testing split was repeated such that each fold became the test fold once, yielding a correlation value for each split. Cross-validation was performed for all methods. The obtained correlations were transformed using Fisher's z-transform, averaged, and the mean z-value was then transformed back into a correlation value using the inverse of Fisher's z-transform.

Results

Simulations

Fig. 4 shows the results of the simulations. In all plots in the figure the recovery of the correlations becomes better as one moves along the x-axis from left to right (i.e. the SNR or the amount of training data increases). In plots (**A**) and (**B**) of that figure, the y-axis indicates the correlation between z and $\tilde{z}$, i.e. the power time course correlation, whereas in plots (**C**) and (**D**) the y-axis indicates the correlation between the true source pattern and the pattern found by the respective method, i.e. the pattern correlation. Please note that all reported correlations are obtained on test data that was not used to train the algorithms.

Plots (**A**) and (**C**) in Fig. 4 display the performance of the methods as a function of SNR. It can be seen, that for higher SNRs all methods have satisfactory performance, i.e. they are able to extract the target power time course from the data with a high degree of correlation. In terms of pattern reconstruction, ICA and the SPoC algorithms reach near perfect performance at high SNR regimes. This metric is not applicable for the regression, because the regression weights cannot be interpreted as the field pattern of a neuronal source.

However, in lower SNR regimes the SPoC algorithms clearly outperform ICA and regression. Comparing the performance of the SPoC methods, we find that the performance of SPoC_{r2} is consistently higher than the performance of SPoC_{λ}. This is true for both performance measures and does not come as a surprise because only SPoC_{r2} is actually optimizing the correlation. The difference in performance between SPoC_{r2} and SPoC_{λ} is strongest in the correlations between z and $\tilde{z}$ in high SNR regimes. In terms of pattern correlation the differences between SPoC_{r2} and SPoC_{λ} are non-negligible but not as pronounced as the differences between the SPoC variants and ICA.

Plots (**B**) and (**D**) in Fig. 4 show the performance of the methods as the amount of training data is varied. The amount of test data is the same for all conditions and the signal-to-noise ratio was fixed to $\gamma = 10^{0.4} \approx 2.5$ (compare with the SNR plot). If only very small amounts of training data are available (i.e. less than 50 epochs), the plots show that SPoC_{r2} is outperformed on the test data by its contestants. In those regimes the algorithm exhibits a tendency to overfit to the training data and consequently it may generalize less well with respect to the test data. However, as more training data becomes available, the performance of the two SPoC algorithms rises faster than ICA and regression. The performance of SPoC_{r2} and SPoC_{λ} is already close to maximum after about 150 to 200 epochs of training data, while the performance of ICA and regression is still considerably lower with the same amount of training data.

Fig. 5 shows the results obtained from a representative simulation run with $\gamma = 10^{0.2} \approx 1.5$. As in the SNR simulations, there were 250 epochs in the training and 600 epochs in the test data. The scalp plot in Fig. 5(A) depicts the true spatial pattern of the simulated target source. Underneath we show as a scalp map the correlations between channel-wise band power time courses and the power time course of the target source. Note how little the correlation pattern resembles the spatial pattern of the simulated source. In Fig. 5(C), the estimated patterns from SPoC_{r2}, SPoC_{λ}, and ICA, as well as the weights of the linear regression are depicted. Regression weights should not be interpreted with respect to the spatial pattern of the source of interest. Yet, they are plotted here in order to make the point explicit. A scatter plot between the true source power time course (z) and the estimated power time courses from the respective methods ($\tilde{z}$) is shown underneath each scalp pattern.

Real EEG data

Fig. 6 depicts the results obtained from the auditory steady state experiment with a slowly changing intensity (i.e. loudness) modulation. Each colored line in the left part of the figure corresponds to a single

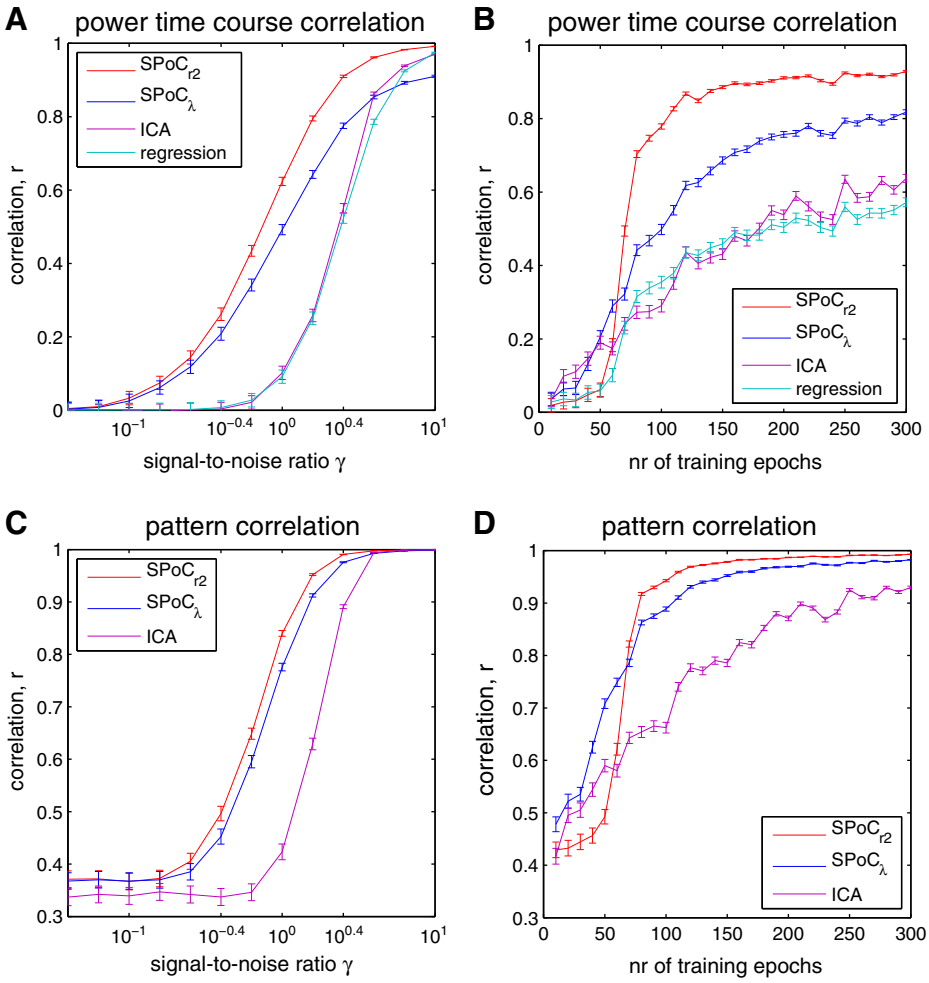

Fig. 4. Simulation results: power time course correlation as a function of signal-to-noise-ratio (A) and as a function of the amount of training data (B). Pattern correlation (similarity between simulated and recovered spatial patterns) as a function of signal-to-noise ratio (C) and as a function of the amount of training data (D). For plots (A) and (C) the number of training epochs was 250. For plots (B) and (D) the SNR was set to $\gamma = 10^{0.4} \approx 2.5$. All correlations are obtained on test data, which was not used for training the algorithms.

participant, while the right part of the figure shows the average across participants. The SPoC algorithms and ICA return several components and therefore the plotted values refer to the cross-validated correlations obtained from the extracted component that had the highest correlation between its power time course and the sound intensity modulation. It can be seen that SPoC$_{r2}$ and SPoC$_{\lambda}$ outperform ICA and regression in

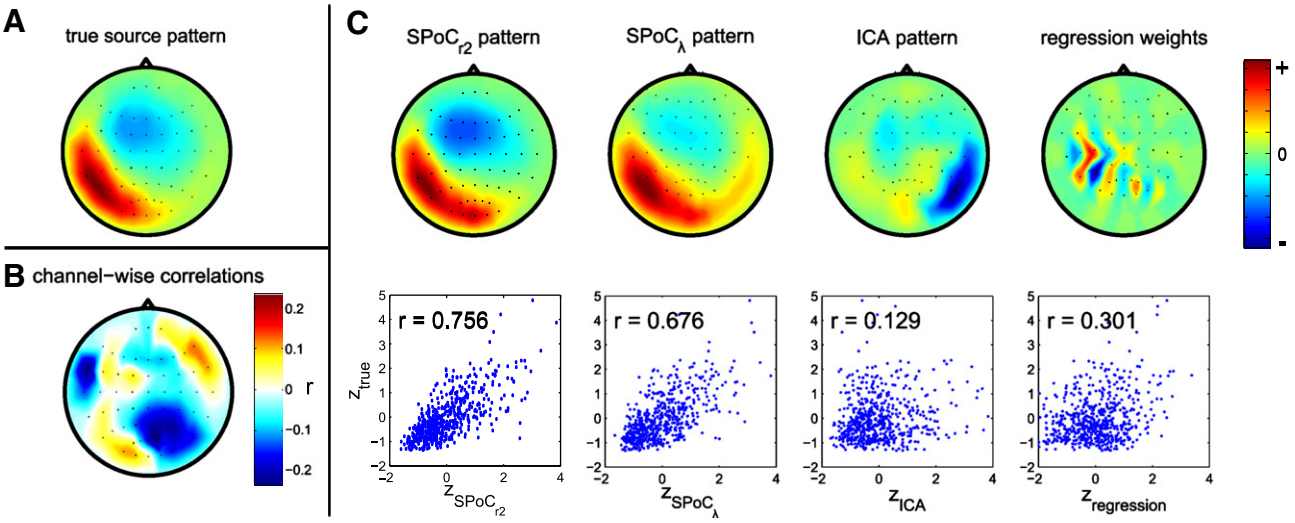

Fig. 5. Simulation results: an example simulation run using 250 training epochs and an SNR of $\gamma = 10^{0.2} \approx 1.5$. (A) The true spatial pattern of the simulated target source. (B) The correlations between channel-wise band power and the band power of the target source, plotted as a scalp map. (C) The scalp patterns of best correlating components and the corresponding scatter plots between true and estimated source power for the different methods.

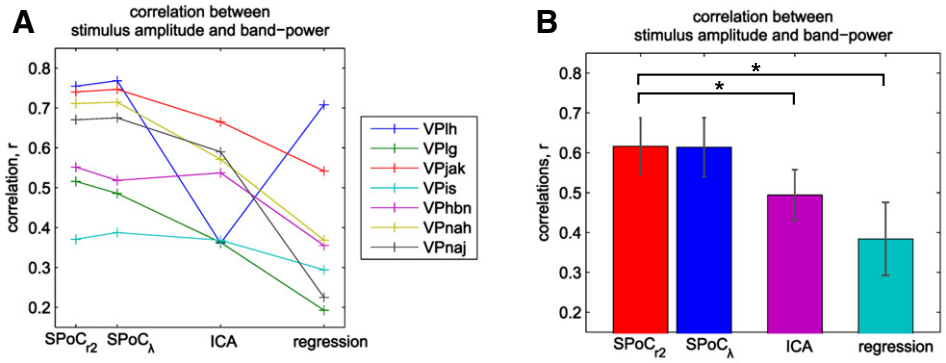

Fig. 6. Real EEG data results: correlation between stimulus intensity and EEG power at the steady state frequency. (A) Each colored line corresponds to a participant and shows the obtained correlations for all methods (mean over cross-validation folds). (B) Same information as in A, averaged over subjects. Error bars depict the standard error of the mean and a black star indicates statistically significant difference at $p < 0.05$.

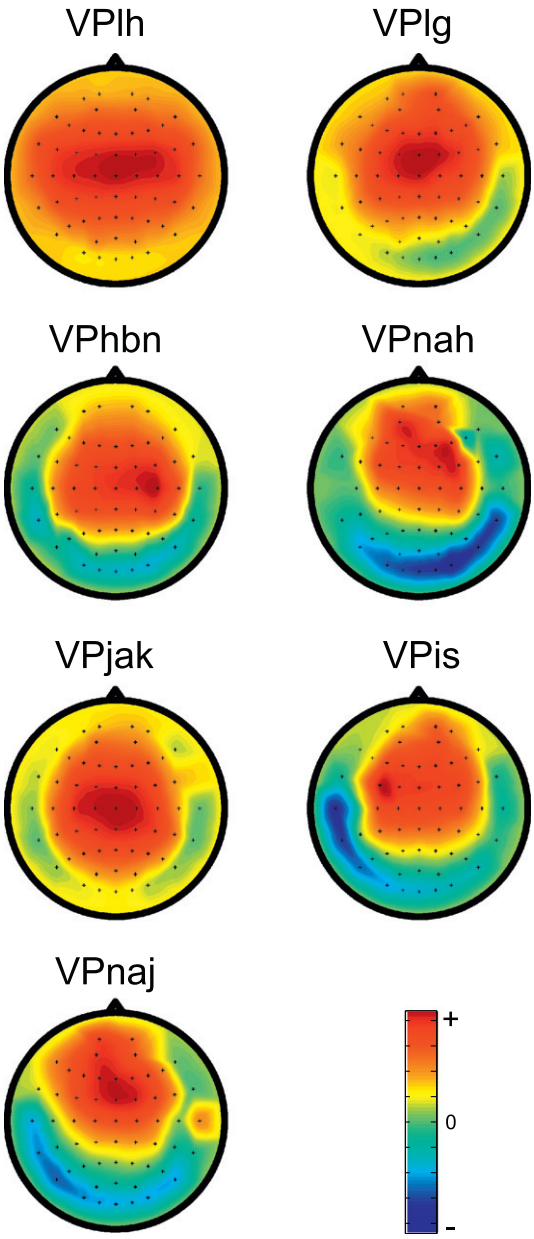

Fig. 7. Real EEG data results: spatial patterns obtained by SPoC$_{r2}$ for each participant. The spatial patterns correspond to the filters that maximize the correlation between power time course and stimulus intensity.

the majority of subjects. The SPoC algorithms yield statistically significant larger correlations between power time courses and the sound intensity modulation than ICA or regression ($p < 0.05$, Wilcoxon rank sum test). Furthermore, on this data set the performance of SPoC$_{\lambda}$ is statistically indistinguishable from the performance of SPoC$_{r2}$.

Fig. 7 shows the spatial patterns (see last paragraph of the Optimizing source power covariance section) corresponding to the best spatial filters for each subject. Best spatial filter here means the spatial filter $\mathbf{w}$ that yielded the largest correlation between the power time course of $\mathbf{w}^{\top}\mathbf{x}$ (i.e. the power time course of the filtered signal) and z. Please note that the polarity of the spatial patterns (as well as of the corresponding filters) is arbitrary. For each pattern, the polarity was set such that the pattern value at EEG electrode Cz is positive.

Fig. 8 shows more detailed results for a representative participant (VPnaj). These plots show channel-wise correlations plotted as a scalp map; the spatial patterns of highest correlating SPoC$_{r2}$, SPoC$_{\lambda}$, and ICA components; as well as the power spectra of a single EEG channel (Fz) and the spectra obtained after spatial filtering with the corresponding SPoC$_{r2}$, SPoC$_{\lambda}$, or ICA filter. Please note that for all subjects the SPoC$_{\lambda}$ filter that maximized the covariance (i.e. the objective function of SPoC$_{\lambda}$) also exhibited the maximal correlation between the power time course and stimulus intensity. It can be seen that the channel-wise correlations are low in magnitude and that the pattern of correlation values shows little resemblance with the components obtained from the spatial filtering methods. Between SPoC$_{r2}$, SPoC$_{\lambda}$, and ICA, the obtained patterns are quite similar, indicating that the same source (or set of sources) has been extracted by the algorithms. The second row of plots in Fig. 8 shows the offset-aligned power spectra of EEG channel Cz and the respective best SPoC$_{r2}$, SPoC$_{\lambda}$, and ICA components (corresponding to the spatial patterns above). The spatial filtering methods show a much clearer peak at the steady-state frequency compared to the individual recording channel. The peak is most pronounced in the component extracted by SPoC$_{r2}$, thus yielding the highest signal-to-noise ratio for this particular participant.

Discussion

We presented a novel approach for the extraction of oscillatory sources showing a comodulation of their power with the target function, the latter being for instance reaction time, hit rate or some physical properties of the sensory stimuli (e.g. intensity). The SPoC approach is the first to explicitly address the problem of component extraction for band power correlation/covariance. Using two implementations of our approach (the SPoC$_{\lambda}$ and the SPoC$_{r2}$ algorithm) we were able to show that it performed better than other methods commonly used for the investigation of a relationship between behavioral measures and a power of oscillations (sensor space regressions, ICA).

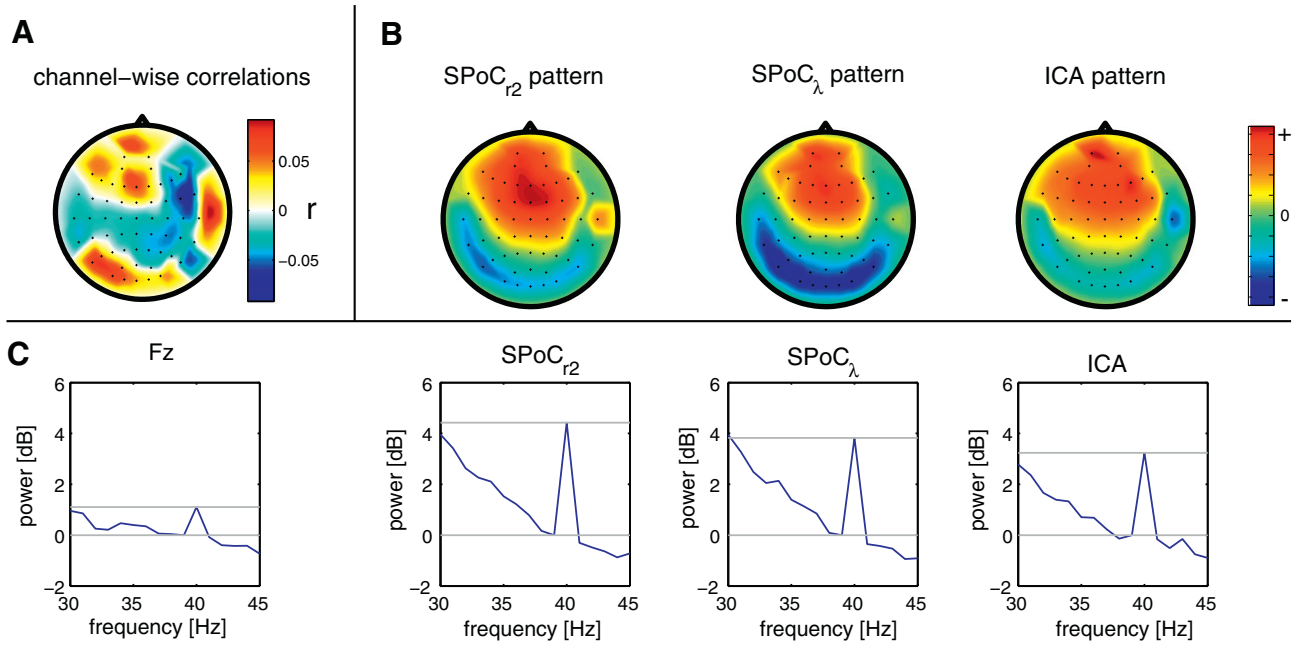

Fig. 8. Real EEG data results: spatial patterns and power spectra for a representative participant (VPnaj). (A) Channel-wise correlation between band power and sound intensity. (B) Spatial patterns of the best SPoC$_{r2}$, SPoC$_{\lambda}$, and ICA component. (C) Offset-aligned power spectra of a single EEG channel (Fz), as well as of the components depicted in the top row. Gray lines in the power spectra plot indicate the difference between power in the 39 Hz and 40 Hz bin, i.e. the signal-to-noise ratio in the spectral domain.

SPoC showed promising results in the extraction of auditory sources generating steady-state responses. The extracted patterns were consistent with ERP-type analysis of auditory steady state responses in the 40 Hz range. Herdman et al. (2002) investigated the source activity underlying the responses to 39 Hz modulated tones. They found a vertically oriented dipolar pattern with maxima (minima) at mid-frontal electrode positions and corresponding minima (maxima) at posterior neck positions, where the sign of minima and maxima depends on the phase of the stimulus. The obtained spatial SPoC patterns corresponded well with the findings of (Herdman et al., 2002).

Comparing the results obtained on the real EEG data to those obtained on the simulated data, we find that the performance differences between SPoC and ICA on the real data are comparable to those found in simulations with moderately high SNR. This indicates that the sources activated in the auditory steady state paradigm are relatively strong compared to background activity in the frequency band of interest. However, the significantly larger correlations obtained with SPoC underline its ability to extract the signal of interest while effectively suppressing unrelated noise sources at the same time. This makes SPoC a valuable tool in scenarios in which the time course of the target variable is to be predicted from ongoing EEG in an online manner.

Below we elaborate on some technical aspects of the SPoC algorithms. If an analysis setting requires the exploration of one or more parameters and thereby multiple runs of the analysis method, then processing speed of the method might be an issue. Some BSS methods require a number of iterations which may take minutes to converge on a standard computer. For a single run only, the range of minutes should not, however, be a problem. However, if the number of runs increases greatly (e.g. for bootstrapping (Meinecke et al., 2002)) minutes can easily become many hours on single processors. Thus it is important to point out that the generalized eigenvalue computation in the SPoC$_{\lambda}$ algorithm takes only fractions of a second, and that is why SPoC$_{\lambda}$ unproblematically allows for (a) extensive parameter studies, or (b) bootstrapping efforts or (c) online evaluations within a time window within only moderate processing time demands.

As a technical side remark we would like to also mention that the SPoC$_{\lambda}$ algorithm is intimately related to the Common Spatial Pattern (CSP) algorithm family (Blankertz et al., 2008). CSP is the current most popular method in Brain–Computer Interface systems, which are based on oscillatory brain signals (Blankertz et al., 2007; Lemm et al., 2011). When the target variable z is binary, classical CSP is obtained as a special case of SPoC$_{\lambda}$. One may thus view SPoC$_{\lambda}$ as a regression extension of CSP to continuous target variables. In such a regression scenario, CSP could still be used but it would require a form of binning of the target variable (e.g. mean- or median split, or using percentiles), which might be arbitrary. Both SPoC algorithms, however, are specifically designed for continuous target variables and therefore do not require such preprocessing.

The SPoC approach is intended to be used on multichannel EEG and MEG data. However, it is not limited to the application of non-invasive imaging methods and should perform equally well for invasive recordings. A specific application scenario for SPoC would be studies with intra-cortical electrodes in epilepsy patients and recordings obtained from deep brain structures such as Globus Pallidus and Subthalamic Nucleus in patients with Parkinson's Disease. In fact, given a special clinical interest in understanding brain mechanisms of the neurological disorders, a precise localization of pathological neuronal networks would be a great advantage, such as for instance in clarifying the neuronal generators of tremor in patients with Parkinson's Disease (Wichmann and Delong, 2011). In this case a tremor can be used as a target variable in order to extract corresponding sources of beta or high-frequency oscillations in the thalamo–cortical–basal network.

Reaction time is a standard and widely used measure in a large number of psychophysiological studies (see for review: Maki and Ilmoniemi (2007) and Meyer et al. (1988)). Often the differences between the studied experimental conditions are very small. Finding associated differences in the power of oscillations is thus quite challenging and therefore refined extraction of task relevant neuronal processes is required. When using SPoC, reaction times can be used as a target variable thus allowing an extraction of task relevant neuronal oscillations. Moreover, given that SPoC provides extraction of both positive and negative correlations one can find oscillatory components showing reciprocal contribution to reaction times. Another important area for SPoC application is research on combined use of EEG and Transcranial Magnetic Stimulation (TMS (Ilmoniemi et al., 1997; Nikulin et al., 2003)). One of the intriguing findings in TMS research is a large variability of Motor Evoked

Potentials (MEPs) produced by the stimulation of the motor cortex. This variability in MEPs most likely reflects changes in cortical excitability, and thus analysis of pre-stimulus oscillatory activity might allow unique opportunity to trace the nature of neuronal processes responsible for changes in excitability. Previous research on this topic has primarily been performed in sensor space (Maki and Ilmoniemi, 2010; Sauseng et al., 2009), where a mixture of multiple sources was a major drawback. The use of SPoC would allow extraction of specific oscillatory sources associated with the changes in cortical excitability. Another scenario where SPoC can be used is for studying cortico-muscular rhythmic interactions. They are usually studied with phase synchronization measures (so called cortico-muscular coherence (Baker, 2007)). However, it becomes increasingly clear that not only phase-to-phase but also amplitude-to-amplitude neuronal interactions (Bayraktaroglu et al., 2013; Daffertshofer and van Wijk, 2011) are important for understanding brain functioning. The use of SPoC would allow studying neuronal sources showing amplitude-to-amplitude interactions, which is indicative of interactions between local dynamics in the cortex and spinal cord (Bayraktaroglu et al., 2013).

The ability to gain understanding about the results of a parameter optimization is an important aspect of machine learning methods (Montavon et al., 2013). Note that SPoC properly implements the commonly accepted generative model of EEG/MEG and therefore it is possible to meaningfully interpret its results within this generative model. This also allows subsequent source localization (Baillet et al., 2001; Haufe et al., 2008, 2011) or further multimodal processing (Bießmann et al., 2011; Fazli et al., 2012) — aspects that we will pursue in a future research effort towards a better understanding of cognitive brain function.

In summary, SPoC is an approach that enables a reliable and fast extraction of neuronal oscillations, whose power time course comodulates with an external target function. Because of SPoC's superiority to other standard techniques, we advocate its use for recovering associations between cognitive/motor variables and neuronal activity.

Acknowledgments

SD, JH, and MT acknowledge funding by the European ICT Programme Project FP7-224631 (TOBI). SD is also supported by GRK 1589/1. FCM gratefully acknowledges support by the German Ministry of Education and Research (BMBF) through the 'Adaptive BCI' Project, FKZ 01GQ1115. SH acknowledges support by the BMBF Grant No. 01GQ0850. KRM acknowledges funding by the World Class University Program through the National Research Foundation of Korea funded by the Ministry of Education, Science, and Technology, under grant R31-10008. VN acknowledges funding by the German Research Foundation (DFG) grant no. KFO 247 and by the Bernstein Center for Computational Neuroscience, Berlin.

Appendix A. Correlating the power of single sensors

Let us for simplicity assume that s is the only source whose power is correlated to the target, and there is only one noise source n, whose power is not correlated to the target. The measurement at electrode k is then expressed as $x_k(t) = a_k s(t) + b_k n$, where a_k and b_k are the respective mixing coefficients. The band power at x_k is given as the variance over time, which simplifies as

$$\begin{aligned} Var[x_k(t)] &= a_k^2 Var[s(t)] + b_k^2 Var[n(t)] \\ &= a_k^2 + b_k^2 \end{aligned}$$

due to the uncorrelatedness and unit variance properties of s and n. Let us now assume the data has been divided up into (subsequent) epochs, and the strengths of the signal and noise sources depend on the epoch. In the following we will adopt the convention that $Var[\cdot]$, $Cov[\cdot]$, and $\mathrm{Corr}[\cdot]$ will be evaluated across the index of their arguments, e.g. $Var[g(t)]$ is the variance of some function g across the time index t and $Cov[g(e), f(e)]$ is the covariance of two functions f and g across epochs. Let $\mathrm{Var}[x_k(t)](e)$ denote the variance of $x_k(t)$ in the epoch with index e, thus making $\mathrm{Var}[x_k](e)$ a function of e. The correlation between $z(e)$ and the band power at channel k across epochs is then given by

$$\mathrm{Corr}[Var[x_k(t)](e), z(e)] = \frac{Cov\left[a_k^2(e) + b_k^2(e), z(e)\right]}{\sqrt{Var\left[a_k^2(e) + b_k^2(e)\right] Var[z(e)]}}. \tag{A.1}$$

Without loss of generality we can assume that $\mathrm{Var}[z(e)] = 1$. Moreover, since the noise power $b_k^2(e)$ is neither correlated to the signal power $a_k^2(e)$ nor to the target $z(e)$,

$$\begin{aligned} &\mathrm{Corr}[Var[x_k(t)](e), z(e)] \\ &= \frac{Cov\left[a_k^2(e), z(e)\right]}{\sqrt{Var\left[a_k^2(e)\right] + Var\left[b_k^2(e)\right]}} \\ &= \frac{Cov\left[a_k^2(e), z(e)\right]}{\sqrt{Var\left[a_k^2(e)\right]}} \cdot \frac{\sqrt{Var\left[a_k^2(e)\right]}}{\sqrt{Var\left[a_k^2(e)\right] + Var\left[b_k^2(e)\right]}} \\ &= \frac{1}{q}\mathrm{Corr}\left[a_k^2(e), z(e)\right] , \end{aligned} \tag{A.2}$$

with

$$q = \sqrt{1 + \frac{Var\left[b_k^2(e)\right]}{Var\left[a_k^2(e)\right]}} . \tag{A.3}$$

That is, the correlation between z and the band power at channel k is the desired correlation between z and the band power of the signal source s normalized by a factor q which depends on the ratio of the band power variation of the signal and noise sources (and hence also indirectly on the strength of the mixing coefficients $a_k^2(e)$ and $b_k^2(e)$). Hence, only for zero noise contribution $b_k(e) = 0, \forall e$ or for zero noise power variation $Var[b_k^2(e)] = 0$ the desired correlation can be recovered. If both these quantities are nonzero, the correlation score will be discounted by a factor which differs for each channel.

Appendix B. Simulated EEG

Simulated EEG data was created using the following steps. Firstly, we generated time courses of $N_{bg} + 1$ hypothetical band-limited EEG sources (1 target source and $N_{bg} + 100$ background sources). For illustrative purposes we chose the α-band as the frequency band of interest, i.e. 8 to 12 Hz. The oscillatory signals were created individually by constructing the amplitude and phase spectrum and then using inverse Fourier transform to obtain the time-domain signal. In the amplitude spectrum, the coefficients of the alpha band were set to 1, whereas the amplitudes of all other frequencies were set to zero. The phase spectrum was chosen randomly for each source time course. Once the time-domain signals were constructed, their envelopes were normalized to 1. Thereafter the signals were multiplied with an amplitude modulation function that consisted of low-pass filtered white noise (filter cut-off below 0.5 Hz). An offset was added such that the slow amplitude modulation was always larger than zero. Squaring the amplitude modulation function of a source yields the power modulation of that source. This constitutes the EEG data in 'source space'.

Physiologically plausible spatial patterns were generated via a realistic EEG forward model (Fonov et al., 2011; Nolte and Dassios, 2005). Specifically, we placed model neural sources (i.e. electrical dipoles, here with randomly chosen orientation) at randomly chosen locations

in 3D voxel space and computed the resulting scalp projections, which we denote with the vector $\mathbf{a}^i \in \mathbb{R}^{N_x}$ for the ith source, where $N_x = 58$ denotes the number of simulated EEG channels. Using these scalp projections, we separately constructed the sensor space representation of the target source (denoted by $\mathbf{x}_t$) and the sensor space representation of background neural activity (denoted by $\mathbf{x}_{bg}$):

$$\mathbf{x}_t(t) = \mathbf{a}^1 s_t(t)$$

$$\mathbf{x}_{bg}(t) = \sum_{i=1}^{N_{bg}} \mathbf{a}^i s_i(t).$$

Additionally we added Gaussian distributed noise (zero mean and unit variance), which is spatially as well as temporally uncorrelated. The noise vector is denoted by $\epsilon(t)$. These three constituents (source signal, background activity and sensor noise) were stored in respective data matrices (e.g. $\mathbf{X}_t = [\mathbf{x}_t(1), \cdots, \mathbf{x}_t(T)]$, where $\mathbf{X}_{bg}$ as well as $\mathbf{X}_\epsilon$ are defined accordingly). Finally, the data matrices were combined according to the following parameterized equation

$$\mathbf{X} = \gamma \mathbf{X}t + \mathbf{X}bg + \frac{\gamma_\epsilon}{\|\mathbf{X}_t\|_F}\mathbf{X}_\epsilon, \tag{B.1}$$

where $\|\mathbf{X}_t\|_F$ denotes the Frobenius norm of the matrix $\mathbf{X}_t$. The parameters γ and γ_ϵ control the relative weightings of the signal constituents: γ_ϵ controls the strength of the sensor noise, while γ controls the strength of the target source. The value of γ_ϵ was fixed to 0.1 for all simulations and the value of γ was varied.

References

Baillet, S., Mosher, J.C.J., Leahy, R.M.R., 2001. Electromagnetic brain mapping. IEEE Signal Process. Mag. 18, 14–30. http://dx.doi.org/10.1109/79.962275.

Baker, S.N., 2007. Oscillatory interactions between sensorimotor cortex and the periphery. Curr. Opin. Neurobiol. 17, 649–655.

Başar, E., Schürmann, M., Başar-Eroglu, C., Karakaş, S., 1997. Alpha oscillations in brain functioning: an integrative theory. Int. J. Psychophysiol. 26, 5–29.

Bauer, M., Oostenveld, R., Peeters, M., Fries, P., 2006. Tactile spatial attention enhances gamma-band activity in somatosensory cortex and reduces low-frequency activity in parieto-occipital areas. J. Neurosci. 26, 490–501. http://dx.doi.org/10.1523/JNEUROSCI.5228-04.2006.

Bayraktaroglu, Z., von Carlowitz-Ghori, K., Curio, G., Nikulin, V.V., 2013. It is not all about phase: amplitude dynamics in corticomuscular interactions. NeuroImage 64, 496–504.

Bießmann, F., Plis, S.M., Meinecke, F.C., Eichele, T., Müller, K.R., 2011. Analysis of multimodal neuroimaging data. IEEE Rev. Biomed. Eng. 4, 26–58.

Blankertz, B., Dornhege, G., Krauledat, M., Müller, K.R., Curio, G., 2007. The non-invasive Berlin brain–computer interface: fast acquisition of effective performance in untrained subjects. NeuroImage 37, 539–550. http://dx.doi.org/10.1016/j.neuroimage.2007.01.051.

Blankertz, B., Tomioka, R., Lemm, S., Kawanabe, M., Müller, K.R., 2008. Optimizing spatial filters for robust EEG single-trial analysis. IEEE Signal Process. Mag. 25, 41–56. http://dx.doi.org/10.1109/MSP.2008.4408441.

Blankertz, B., Sannelli, C., Halder, S., Hammer, E.M., Kübler, A., Müller, K.R., Curio, G., Dickhaus, T., 2010. Neurophysiological predictor of SMR-based BCI performance. NeuroImage 51, 1303–1309. http://dx.doi.org/10.1016/j.neuroimage.2010.03.022.

Blankertz, B., Lemm, S., Treder, M., Haufe, S., Müller, K.R., 2011. Single-trial analysis and classification of ERP components — a tutorial. NeuroImage 56, 814–825. http://dx.doi.org/10.1016/j.neuroimage.2010.06.048.

Brovelli, A., Lachaux, J.P., Kahane, P., Boussaoud, D., 2005. High gamma frequency oscillatory activity dissociates attention from intention in the human premotor cortex. NeuroImage 28, 154–164. http://dx.doi.org/10.1016/j.neuroimage.2005.05.045.

Buzsáki, G., Draguhn, A., 2004. Neuronal oscillations in cortical networks. Science (New York, N.Y.) 304, 1926–1929. http://dx.doi.org/10.1126/science.1099745.

Colgin, L.L., Denninger, T., Fyhn, M., Hafting, T., Bonnevie, T., Jensen, O., Moser, M.B., Moser, E.I., 2009. Frequency of gamma oscillations routes flow of information in the hippocampus. Nature 462, 353–357. http://dx.doi.org/10.1038/nature08573.

Daffertshofer, A., van Wijk, B.C.M., 2011. On the influence of amplitude on the connectivity between phases. Front. Neuroinform. 5, 6.

Darchia, N., Campbell, I., Tan, X., Feinberg, I., 2007. Kinetics of NREM delta EEG power density across NREM periods depend on age and on delta-band designation. Sleep 30, 71–79.

Debener, S., Herrmann, C.A.C.S., Kranczioch, C., Gembris, D., Engel, A.K., 2003. Top–down attentional processing enhances auditory evoked gamma band activity. NeuroReport 14, 683–686. http://dx.doi.org/10.1097/01.wnr.0000064987.

Demanuele, C., Broyd, S.J., Sonuga-Barke, E.J.S., James, C., 2012. Neuronal oscillations in the EEG under varying cognitive load: a comparative study between slow waves and faster oscillations. Clin. Neurophysiol. 124, 247–262.

Fazli, S., Mehnert, J., Steinbrink, J., Curio, G., Villringer, A., Müller, K.R., Blankertz, B., 2012. Enhanced performance by a hybrid NIRS–EEG brain computer interface. NeuroImage 59, 519–529.

Fonov, V., Evans, A.C., Botteron, K., Almli, C.R., McKinstry, R.C., Collins, D.L., 2011. Unbiased average age-appropriate atlases for pediatric studies. NeuroImage 54, 313–327.

Galambos, R., Makeig, S., Talmachoff, P.J., 1981. A 40-Hz auditory potential recorded from the human scalp. Proc. Natl. Acad. Sci. U. S. A. 78, 2643–2647.

Gevins, A., Leong, H., Du, R., Smith, M.E., Le, J., DuRousseau, D., Zhang, J., Libove, J., 1995. Towards measurement of brain function in operational environments. Biol. Psychol. 40, 169–186.

Gonzalez Andino, S.L., Michel, C.M., Thut, G., Landis, T., Grave de Peralta, R., 2005. Prediction of response speed by anticipatory high-frequency (gamma band) oscillations in the human brain. Hum. Brain Mapp. 24, 50–58. http://dx.doi.org/10.1002/hbm.20056.

Grosse-Wentrup, M., Schölkopf, B., Hill, J., 2011. Causal influence of gamma oscillations on the sensorimotor rhythm. NeuroImage 56, 837–842. http://dx.doi.org/10.1016/j.neuroimage.2010.04.265.

Haegens, S., Händel, B.F., Jensen, O., 2011a. Top–down controlled alpha band activity in somatosensory areas determines behavioral performance in a discrimination task. J. Neurosci. 31, 5197–5204. http://dx.doi.org/10.1523/JNEUROSCI.5199-10.2011.

Haegens, S., Nácher, V., Hernández, A., Luna, R., Jensen, O., Romo, R., 2011b. Beta oscillations in the monkey sensorimotor network reflect somatosensory decision making. Proc. Natl. Acad. Sci. U. S. A. 108, 10708–10713. http://dx.doi.org/10.1073/pnas.1107297108.

Hari, R., Hämäläinen, M., Joutsiniemi, S.L., 1989. Neuromagnetic steady-state responses to auditory stimuli. J. Acoust. Soc. Am. 86, 1033–1039.

Haufe, S., Nikulin, V.V., Ziehe, A., Müller, K.R., Nolte, G., 2008. Combining sparsity and rotational invariance in EEG/MEG source reconstruction. NeuroImage 42, 726–738.

Haufe, S., Tomioka, R., Dickhaus, T., Sannelli, C., Blankertz, B., Nolte, G., Müller, K.R., 2011. Large-scale EEG/MEG source localization with spatial flexibility. NeuroImage 54, 851–859. http://dx.doi.org/10.1016/j.neuroimage.2010.09.003.

Herdman, A.T., Lins, O., Van Roon, P., Stapells, D.R., Scherg, M., Picton, T.W., 2002. Intracerebral sources of human auditory steady-state responses. Brain Topogr. 15, 69–86.

Holm, A., Lukander, K., Korpela, J., Sallinen, M., Müller, K.M.I., 2009. Estimating brain load from the EEG. Sci. World J. 9, 639–651. http://dx.doi.org/10.1100/tsw.2009.83.

Ilmoniemi, R.J., Virtanen, J., Ruohonen, J., Karhu, J., Aronen, H.J., Näätänen, R., Katila, T., 1997. Neuronal responses to magnetic stimulation reveal cortical reactivity and connectivity. Neuroreport 8, 3537–3540.

Jensen, O., Kaiser, J., Lachaux, J.P., 2007. Human gamma-frequency oscillations associated with attention and memory. Trends Neurosci. 30, 317–324. http://dx.doi.org/10.1016/j.tins.2007.05.001.

Jin, Y., OHalloran, J.P., Plon, L., Sandman, C.A., Potkin, S.G., 2006. Alpha EEEG predicts visual teaction time. Int. J. Neurosci. 116, 1035–1044. http://dx.doi.org/10.1080/00207450600553232.

John, M.S., Dimitrijevic, A., Picton, T.W., 2003. Efficient stimuli for evoking auditory steady-state responses. Ear Hear. 24, 406–423. http://dx.doi.org/10.1097/01.AUD.0000090442.37624.BE.

Kaiser, J., Hertrich, I., Ackermann, H., Lutzenberger, W., 2006. Gamma-band activity over early sensory areas predicts detection of changes in audiovisual speech stimuli. NeuroImage 30, 1376–1382. http://dx.doi.org/10.1016/j.neuroimage.2005.10.042.

Klimesch, W., 1999. EEG alpha and theta oscillations reflect cognitive and memory performance: a review and analysis. Brain Res. Rev. 29, 169–195.

Klimesch, W., Doppelmayr, M., Russegger, H., Pachinger, T., Schwaiger, J., 1998. Induced alpha band power changes in the human EEG and attention. Neurosci. Lett. 244, 73–76.

Lemm, S., Blankertz, B., Dickhaus, T., Müller, K.R., 2011. Introduction to machine learning for brain imaging. NeuroImage 56, 387–399. http://dx.doi.org/10.1016/j.neuroimage.2010.11.004.

Maeder, C.L., Sannelli, C., Haufe, S., Blankertz, B., 2012. Prestimulus sensorimotor rhythms influence brain–computer interface classification performance. IEEE Trans. Neural Syst. Rehabil. Eng. 20, 653–662.

Makeig, S., Jung, T.P., 1996. Tonic, phasic, and transient EEG correlates of auditory awareness in drowsiness. Cogn. Brain Res. 4, 15–25.

Maki, H., Ilmoniemi, R.J., 2007. What, when, where in the brain? Exploring mental chronometry with brain imaging and electrophysiology. Rev. Neurosci. 18, 159–171.

Maki, H., Ilmoniemi, R.J., 2010. The relationship between peripheral and early cortical activation induced by transcranial magnetic stimulation. Neurosci. Lett. 478, 24–28.

Meinecke, F., Ziehe, A., Kawanabe, M., Müller, K.R., 2002. A resampling approach to estimate the stability of one-dimensional or multidimensional independent components. IEEE Trans. Biomed. Eng. 49, 1514–1525. http://dx.doi.org/10.1109/TBME.2002.805480.

Meyer, D.E., Osman, A.M., Irwin, D.E., Yantis, S., 1988. Modern mental chronometry. Biol. Psychol. 26, 3–67.

Montavon, G., Braun, M.L., Krueger, T., Müller, K.-R., 2013. Analyzing local structure in Kernel-based learning: explanation, complexity and reliability assessment. Signal Processing Magazine, IEEE 30 (4), 62–74. http://dx.doi.org/10.1109/MSP.2013.2249294.

Nikulin, V.V., Kicic, D., Kähkönen, S., Ilmoniemi, R.J., 2003. Modulation of electroencephalographic responses to transcranial magnetic stimulation: evidence for changes in cortical excitability related to movement. Eur. J. Neurosci. 18, 1206–1212.

Nolte, G., Dassios, G., 2005. Analytic expansion of the EEG lead field for realistic volume conductors. Phys. Med. Biol. 50, 3807–3823.

Nunez, P.L., Srinivasan, R., 2006. Electric Fields of the Brain: The Neurophysics of EEG, vol. 35. Oxford University Press. http://dx.doi.org/10.1063/1.2915137.

Osipova, D., Takashima, A., Oostenveld, R., Fernández, G., Maris, E., Jensen, O., 2006. Theta and gamma oscillations predict encoding and retrieval of declarative memory. J. Neurosci. 26, 7523–7531. http://dx.doi.org/10.1523/JNEUROSCI.1948-06.2006.

Parra, L.C., Spence, C.D., Gerson, A.D., Sajda, P., 2005. Recipes for the linear analysis of EEG. NeuroImage 28, 326–341. http://dx.doi.org/10.1016/j.neuroimage.2005.05.032.
Picton, T.W., John, M.S., Dimitrijevic, A., Purcell, D., 2003. Human auditory steady-state responses. Int. J. Audiol. 42, 177–219.
Plourde, G., Stapells, D.R., Picton, T.W., 1991. The human auditory steady-state evoked potentials. Acta Otolaryngol. 491, 153–160.
Rieder, M.K., Rahm, B., Williams, J.D., Kaiser, J., 2011. Human γ—band activity and behavior. Int. J. Psychophysiol. 79, 39–48. http://dx.doi.org/10.1016/j.ijpsycho.2010.08.010.
Rodriguez, R., Picton, T., Linden, D., Hamel, G., Laframboise, G., 1986. Human auditory steady state responses: effects of intensity and frequency. Ear Hear. 7, 300–313.
Romei, V., Brodbeck, V., Michel, C., Amedi, A., Pascual-Leone, A., Thut, G., 2008. Spontaneous fluctuations in posterior alpha-band EEG activity reflect variability in excitability of human visual areas. Cereb. Cortex 18, 2010–2018. http://dx.doi.org/10.1093/cercor/bhm229.
Sauseng, P., Klimesch, W., Gerloff, C., Hummel, F.C., 2009. Spontaneous locally restricted EEG alpha activity determines cortical excitability in the motor cortex. Neuropsychologia 47, 284–288. http://dx.doi.org/10.1016/j.neuropsychologia.2008.07.021.
Tallon-Baudry, C., Bertrand, O., Hénaff, M.A., Isnard, J., Fischer, C., 2005. Attention modulates gamma-band oscillations differently in the human lateral occipital cortex and fusiform gyrus. Cereb. Cortex 15, 654–662. http://dx.doi.org/10.1093/cercor/bhh167.
Thut, G., Nietzel, A., Brandt, S.A., Pascual-Leone, A., 2006. Alpha-band electroencephalographic activity over occipital cortex indexes visuospatial attention bias and predicts visual target detection. J. Neurosci. 26, 9494–9502. http://dx.doi.org/10.1523/JNEUROSCI.0875-06.2006.
Wichmann, T., Delong, M.R., 2011. Deep-brain stimulation for basal ganglia disorders. Basal Ganglia 1, 65–77. http://dx.doi.org/10.1016/j.baga.2011.05.001.
Womelsdorf, T., Fries, P., 2007. The role of neuronal synchronization in selective attention. Curr. Opin. Neurobiol. 17, 154–160. http://dx.doi.org/10.1016/j.conb.2007.02.002.